iScience

CellPress
OPEN ACCESS

Article

$GABA_{B1e}$ promotes the malignancy of human cancer cells by targeting the tyrosine phosphatase PTPN12

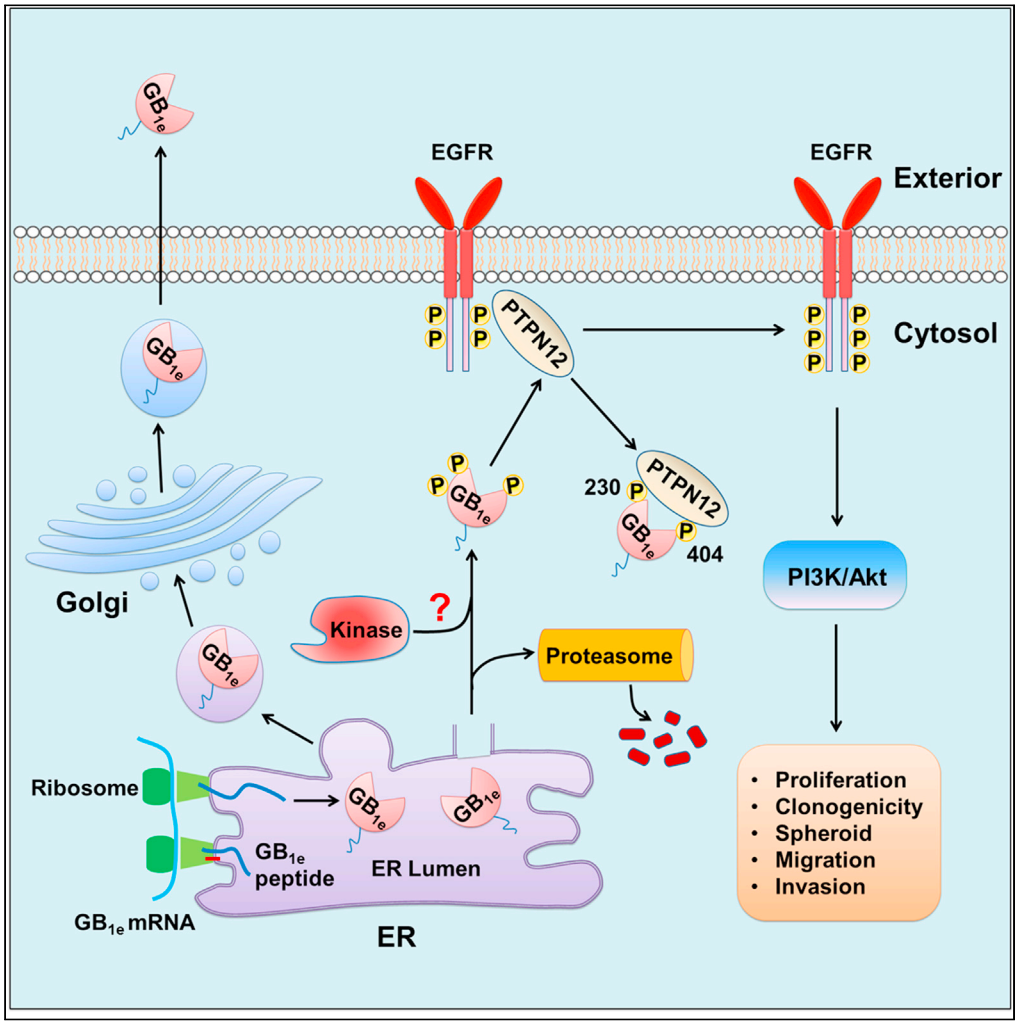

Bo Wei, Yini Zhu, Peng Yang, ..., Jean-Philippe Pin, Xinnong Jiang, Jianfeng Liu

jiangxn88@hust.edu.cn (X.J.)
jfliu@mail.hust.edu.cn (J.L.)

Highlights

$GABA_{B1e}$ promotes the malignancy of breast cancer cells both *in vitro* and *in vivo*

Specific phosphorylation of $GABA_{B1e}$ is critical for its association with PTPN12

$GABA_{B1e}$ disrupts EGFR interacting with PTPN12 and induces EGFR-PI3K/Akt signaling

Wei et al., iScience *24*, 103311
November 19, 2021
https://doi.org/10.1016/j.isci.2021.103311

iScience

CellPress
OPEN ACCESS

Article

$GABA_{B1e}$ promotes the malignancy of human cancer cells by targeting the tyrosine phosphatase PTPN12

Bo Wei,[1,6] Yini Zhu,[1,6] Peng Yang,[2] Yong Han,[3] Suyun Wang,[1] Xiaomei Wang,[1] Shuai Xia,[1] Xiaoguang Song,[1] Zhongling Zhang,[1] Sheng Wang,[4] Philippe Rondard,[5] Jean-Philippe Pin,[5] Xinnong Jiang,[1,*] and Jianfeng Liu[1,7,*]

SUMMARY

Neurotransmitter receptors are involved in cancer progression. Among them, the heterodimeric $GABA_B$ receptor, activated by the main inhibitory neurotransmitter GABA, is composed of the transmembrane $GABA_{B1}$ and $GABA_{B2}$ subunits. The oncogenic role of the isoform $GABA_{B1e}$ (GB_{1e}) containing only the extracellular domain of $GABA_{B1}$ remains unclear. We revealed that GB_{1e} is largely expressed in human breast cancer (BrCa) cell lines as well as in BrCa tissues where it is upregulated. Moreover, GB_{1e} promoted the malignancy of BrCa cells both *in vitro* and *in vivo*. We propose that GB_{1e} favors EGFR signaling by interacting with PTPN12 to disrupt the interaction between EGFR and PTPN12, and phosphorylation of Y230 and Y404 on GB_{1e} is required in this process. Our data highlight that the *GABBR1* gene through the expression of the GB_{1e} isoform might play an important oncogenic role in BrCa and that GB_{1e} is of interest for the treatment of some cancers.

INTRODUCTION

Breast cancer (BrCa) is the most commonly diagnosed cancer and the leading cause of cancer death among women worldwide, with an estimation of nearly 2.3 million new cases and 685,000 deaths in 2020 (Sung et al., 2021). Although significant improvements have been made in BrCa diagnosis and treatment, it remains the leading cause of cancer death in women (Neophytou et al., 2018). It is therefore critical to identify new potential targets for the treatment of BrCa.

Neurotransmitter receptors are involved in cancer progression due to the modulatory effects of neurotransmitter on cancer cells (Schuller, 2008). The metabotropic receptor for the main inhibitory neurotransmitter gamma-aminobutyric acid (GABA) (Gassmann and Bettler, 2012), i.e. $GABA_B$ receptor, plays a controversial role in cancer cell growth, migration, invasion, and tumorigenesis. $GABA_B$ receptor agonists significantly reduced the incidence and number of gastric cancers in rats (Tatsuta et al., 1990), decreased the migration and metastasis of colon cancer in mice (Joseph et al., 2002; Thaker et al., 2005), inhibited the growth of human hepatocellular carcinoma cells both *in vitro* and *in vivo* (Wang et al., 2008), and reduced the growth of cholangiocarcinoma cells (Fava et al., 2005; Huang et al., 2013). In contrast, other studies revealed that $GABA_B$ receptor activation promoted the invasive ability of prostate and renal cancer cells (Azuma et al., 2003; Inamoto et al., 2007) and the metastasis of mouse breast 4T1 cancer cells (Zhang et al., 2014). We have also recently reported that $GABA_B$ receptor induced epidermal growth factor (EGFR) transactivation and promoted the invasion of human prostate cancer cells (Xia et al., 2017).

$GABA_B$ receptor is a G-protein-coupled receptor (GPCR) and is composed of $GABA_{B1}$ (GB_1) and $GABA_{B2}$ (GB_2) subunits (Pin et al., 2004), encoded by the *GABBR1* and *GABBR2* genes, respectively. GB_1 has at least 14 isoforms (GB_{1a-n}), among which GB_{1a} and GB_{1b} are the most abundant isoforms predominantly expressed in central nervous system (Jiang et al., 2012). $GB_{1a/b}$ contains a large N-terminal extracellular domain (ECD) responsible for GABA, agonist and antagonist binding, a seven-transmembrane domain (TMD), and a C-terminal intracellular region. But the activation of the G protein is mediated by the TMD of GB_2 (Bettler et al., 2004; Pin and Bettler, 2016). Of interest, GB_{1e} is a truncated GB_1 isoform resulting from the alternative splicing of *GABBR1* gene, and it contains only the GB_{1a} ECD ended by nine extra C-terminal residues. GB_{1e} is predominantly transcribed in human and rat peripheral tissues (Mizuta et al., 2008; Schwarz et al., 2000), but its function remains unknown.

[1]Key Laboratory of Molecular Biophysics of MOE, International Research Center for Sensory Biology and Technology of MOST, College of Life Science and Technology, Huazhong University of Science and Technology (HUST), Wuhan 430074, China

[2]Department of Breast & Endocrine Surgery, Union Hospital, Tongji Medical College, Huazhong University of Science and Technology (HUST), Wuhan 430022, China

[3]Department of Pharmacy, Union Hospital, Tongji Medical College, Huazhong University of Science and Technology (HUST), Wuhan 430022, China

[4]Key Laboratory of Molecular Biophysics of MOE, College of Life Science and Technology, Huazhong University of Science and Technology (HUST), Wuhan 430074, China

[5]Institut de Génomique Fonctionnelle (IGF), Université de Montpellier, CNRS, INSERM, 34094 Montpellier, France

[6]These authors contributed equally

[7]Lead contact

*Correspondence: jiangxn88@hust.edu.cn (X.J.), jfliu@mail.hust.edu.cn (J.L.)

https://doi.org/10.1016/j.isci.2021.103311

In this study, we demonstrate that GB_{1e} promotes the malignancy of human BrCa cells both *in vitro* and *in vivo*. GB_{1e} is the predominant GB_1 isoform, and it is upregulated in various human BrCa cell lines and tissues. Its expression level correlates with the tumorigenic potential of BrCa cell lines. Interestingly, GB_{1e} is retrotranslocated from the ER lumen to the cytosol, where it undergoes proteasomal degradation or tyrosine phosphorylation. Phosphorylation of Y230 and Y404 on GB_{1e} is critical for GB_{1e} to hijack the protein tyrosine phosphatase non-receptor type 12 (PTPN12) from EGFR, which in turn promotes cancer cells growth and invasion. Our finding provides a new view for the treatment of BrCa by targeting the interactions between GB_{1e}, PTPN12 and EGFR.

RESULTS

GB_{1e} is abundant in human BrCa cell lines and tissues

GB_{1e}, containing only the ECD of GB_{1a} (Figures 1A and S1A), has been reported to be the predominant GB_1 transcript in human and rat peripheral tissues (Schwarz et al., 2000). Our reverse-transcriptase PCR (RT-PCR) results showed that GB_{1e} transcript (420 bps) was transcribed at different levels in the normal breast MCF10A cells and eight human BrCa cell lines representing major breast cancer subtypes, i.e. estrogen receptor $(ER)^+$/progesterone receptor $(PR)^+$ (MCF7 and T-47D), $Her2^+$ (BT474, AU565, and SK-BR-3), and $ER^-/PR^-/Her2^-$ or triple negative (MDA-MB-453, MDA-MB-231, and BT-549) cell lines. As a negative control, $GB_{1a/b}$ transcript (570 bps) was only detected in cerebellar granule neurons (CGNs) (Figures 1B and S1B). Quantitative RT-PCR using GB_{1e}-specific primers showed that highly tumorigenic MDA-MB-231 and BT-549 cells had higher levels of GB_{1e} mRNA compared with the poorly tumorigenic MCF7 and T-47D cells (Figures S1B and S2).

The expression of GB_{1e} protein in BrCa cell lines was assessed by immunoblotting with a monoclonal antibody recognizing the N-terminal sequence of GB_1. GB_{1e} protein (~78 kDa) was detected in all of the eight BrCa cell lines as well as in MCF-10A cells. Interestingly, higher level of GB_{1e} protein was detected in BrCa cell lines with higher tumorigenic potential (Figures 1C and 1D). As a negative control, GB_{1a} protein (~130 kDa) was only detected in CGNs.

We next examined the expression of GB_{1e} mRNA and protein in 36 BrCa specimens and the matched para-cancerous tissues. Although GB_{1e} transcript was the primary product in both BrCa and para-cancerous tissues, the average levels of GB_{1e} transcript and protein were significantly higher in cancer specimens than those in para-cancerous tissues (Figures 1E, 1F, and S3). Moreover, cancer specimen was intensively immunostained with GB_1 antibody, whereas the para-cancerous tissue was moderately stained (Figure 1G).

Collectively, different expression level of GB_{1e} was detected in both human BrCa cell lines and tissues, and this GB_{1e} level correlates with the tumorigenic potential of BrCa cell lines.

GB_{1e} is secreted and retrotranslocated to the cytosol

We investigated the cellular distribution and secretion of GB_{1e}. In MCF7 cells transfected with the Flag-tagged GB_{1e} (MCF7-GB_{1e}), GB_{1e} was detected at the cell surface and in the cytoplasm, before and after cell membrane permeabilization, respectively (Figure S4A). The majority of GB_{1e} was distributed in the cytoplasm as shown by the lower Flag signal under nonpermeabilized conditions (Figure 2A). GB_{1e} was also secreted to the medium as revealed by the immunoblotting analysis of conditioned medium (CM) with an anti-GB_1 antibody (Figure 2B). Of note, endogenous GB_{1e} was also detected in the cells transfected with the empty plasmid. Two bands corresponding to ~100 and ~78 kDa were detected only in the CM but not in the total cell lysates (TCLs) where only the ~78 kDa was detected. We proposed that this 78 kDa band corresponds to glycosylated GB_{1e} that could be secreted but also be present in the cytosol. In contrast, the secreted 100 kDa protein corresponds to a full glycosylated GB_{1e}, with posttranslational modifications that occur in both ER and Golgi apparatus. This hypothesis is validated by the treatment of the cells with tunicamycin, an inhibitor of protein N-glycosylation, that resulted in one band of GB_{1e} at ~65 kDa in the TCLs, whereas no band was detected in the CM (Figure 2C). We also treated the cells with brefeldin A, a compound disrupting the structure and function of the Golgi apparatus, and the results showed that the intensities of both ~100 and ~78 kDa bands in the CM were strongly reduced, whereas that of ~78 kDa in the TCLs was slightly increased (Figure 2D). These observations suggest that GB_{1e} is modified by N-glycosylation, which occurs in both ER and Golgi apparatus.

Endoplasmic reticulum (ER) is a major site of protein synthesis, and increased protein synthesis may induce ER stress and then the retrotranslocation of proteins from the ER lumen to the cytosol, where proteins

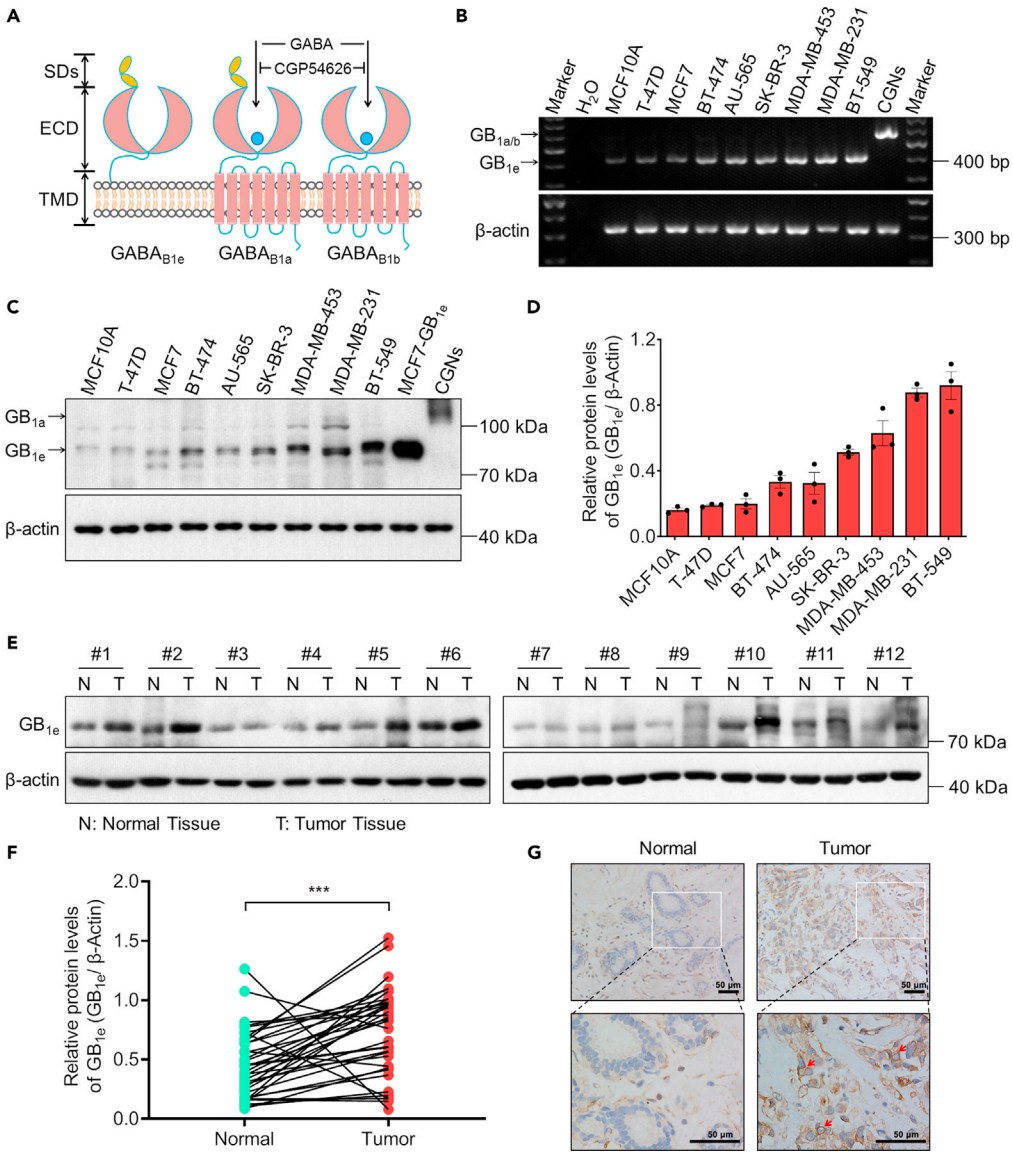

Figure 1. GB$_{1e}$ is abundant in human BrCa cell lines and tissues

(A) The schematic structure of GB$_{1e}$, GB$_{1a}$, and GB$_{1b}$. SD, sushi domain; ECD, extracellular domain; TMD, transmembrane domain.

(B) mRNAs were isolated from the indicated human BrCa cell lines and subjected to RT-PCR analysis. Amplicons representing GB$_{1a/b}$ and GB$_{1e}$ were amplified by using the same primer pairs. Cerebellar granule neurons (CGNs) were used as the positive control for GB$_{1a/b}$ expression. β-actin was used as an internal control.

(C) Immunoblot analysis of GB$_{1e}$ in the indicated BrCa cell lines. MCF7 cells overexpressing GB$_{1e}$ (MCF7-GB$_{1e}$) and CGNs were used as positive controls for GB$_{1e}$ and GB$_{1a}$, respectively. β-actin was used as a loading control.

(D) Quantitative histograms of GB$_{1e}$ expression shown in panel (C). Fold changes of GB$_{1e}$ expression was normalized to β-actin. The data are presented as mean ± SEM (n = 3).

(E) Immunoblot analysis of GB$_{1e}$ in human representative BrCa and tumor adjacent tissues. β-actin was used as a loading control.

(F) Quantitative plot of GB$_{1e}$ expression normalized to β-actin. The data are presented as mean ± SEM (n = 3) and analyzed by unpaired t test. ***$p < 0.001$.

(G) Immunohistochemical analysis of paraffin sections of human BrCa and tumor adjacent tissues with an anti-GB$_1$ antibody. Scale bar, 50 μm.

See also Figures S1, S2, S3 and S11.

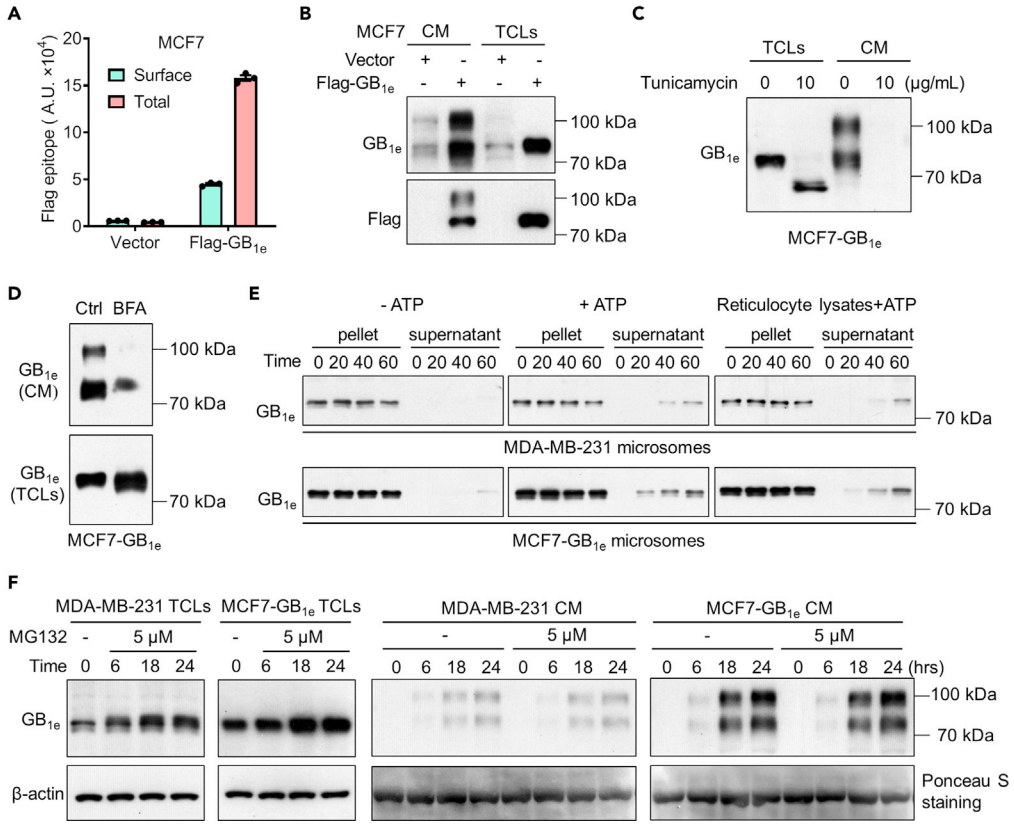

Figure 2. GB_{1e} is secreted and retrotranslocated to the cytosol

(A) ELISA measuring the cell surface and total GB_{1e} in MCF7 cells transfected with Flag-GB_{1e} or vector by using an anti-Flag antibody.

(B) Amounts of GB_{1e} in the concentrated conditioned medium (CM) and total cell lysates (TCLs) from vector or Flag-GB_{1e}-transfected MCF7 cells by immunoblotting with antibodies against GB_1 and Flag.

(C and D) GB_{1e}-transfected MCF7 (MCF7-GB_{1e}) cells were treated or not with 10 μg/mL tunicamycin (C) or 30 μM brefeldin A (BFA) (D) overnight at 37°C. GB_{1e} levels in the TCLs and CM were analyzed by immunoblotting with an anti-GB_1 antibody.

(E) Export assay. (Left and middle panels) Microsomes were resuspended in cold PBS and mixed with 2-fold export buffer with or without ATP. (Right panel) Microsomes were resuspended in 50% reticulocyte lysate diluted with export buffer plus ATP. The mixtures were incubated for the indicated times at 30°C followed by centrifugation. The pellets and supernatants were subjected to immunoblot analysis with an anti-GB_1 antibody.

(F) MDA-MB-231 and MCF7-GB_{1e} cells were treated or not with the proteasome inhibitor MG132 (5 μM) for the indicated times. The TCLs and CM were analyzed by immunoblotting with an anti-GB_1 antibody. β-actin was used as a loading control for the TCL samples. Ponceau S solution was used to stain the membrane to assure equal protein loading of CM samples.

See also Figure S4.

undergo proteasomal degradation (Qu et al., 2021). It has been reported that ER-derived microsomes, containing the retrotranslocon channel that pulls proteins from the ER lumen at the expense of ATP, could be used to study protein export as a cell-free system *in vitro* (Schmitz et al., 2000; Wahlman et al., 2007). To investigate whether GB_{1e} is retrotranslocated to the cytosol in BrCa cells with high GB_{1e} expression, microsomes were isolated from MCF7 cells transfected with GB_{1e} and from MDA-MB-231 cells with high level of endogenous GB_{1e}. The purity and integrity of the isolated microsomes were indicated by the enrichment of the ER marker calnexin (Figure S4B). Trypsin treatment resulted in no degradation of microsomal GB_{1e} in the absence of Triton X-100, but its complete degradation was detected in the presence of Triton X-100, indicating that GB_{1e} is located within the microsomal lumen and no GB_{1e} is attached to the outer surface of the microsomal membranes (Figure S4C). In the protein export assay, microsomes were resuspended in export buffer with or without ATP. The results showed that GB_{1e} was detected in the microsome pellet but barely detectable in the supernatant in the absence of ATP. However, a time-dependent increase of GB_{1e}

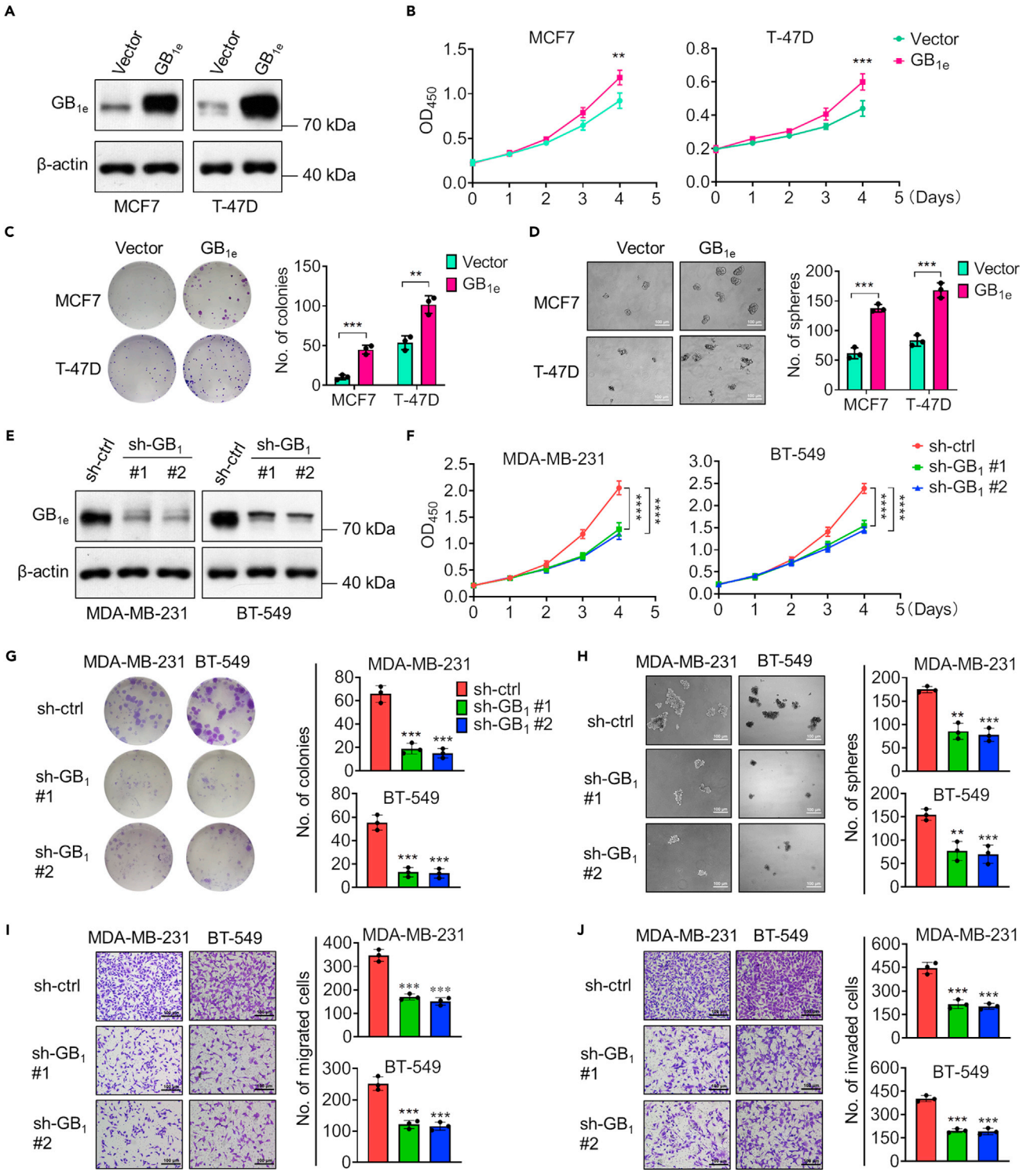

Figure 3. GB_{1e} promotes the malignancy of human BrCa cells *in vitro*

(A–D) MCF7 and T-47D cells were stably transfected with GB_{1e} or vector. (A) Immunoblot analysis assessing the amounts of GB_{1e} with β-actin used as a loading control. (B) Cell proliferation was measured by adding CCK-8 solution to each well 24, 48, 72, or 96 h after cell plating in a 24-well plate (2×10^4 cells/well). (C) Clonogenic assay in which 200 cells were seeded into 24-well plates and cultured for 10–14 days with medium replacement for every 3 days. Colonies visible to the naked eyes were fixed and stained. Representative images were captured (left panel), and the numbers of colonies were counted (right panel). (D) Spheroid formation assay in which 2×10^4 cells were seeded into ultra-low attachment 24-well plates and cultured for 10–14 days.

Figure 3. *Continued*

Representative images were captured (left panel), and the numbers of spheroids was counted (right panel). The data are presented as mean ± SEM (n = 3) and analyzed by unpaired t test (B–D); **p < 0.01, ***p < 0.001, ****p < 0.0001. Scale bar, 100 μm.

(E–J) MDA-MB-231 and BT-549 cells stably transfected with sh-GB_1 #1, #2, or sh-ctrl (control shRNA). (E) Immunoblot of GB_{1e} with β-actin used as a loading control. (F) Cell proliferation assessed by CCK-8 solution. (G and H) Clonogenic (G) and spheroid formation (H) assays. Representative images of colonies and spheres (left panels) formed by the indicated cells and quantification of the numbers of colonies and spheres (right panels) are shown. (I and J) Transwell assay in which cells were added to the upper chamber and incubated at 37°C for 24 h. Cells on the bottom surface of the membrane were fixed and stained. Representative images of cell migration (I) and invasion (J) were shown, and the numbers of migrated and invaded cells were quantitated. All experiments were performed in triplicates. The data are presented as mean ± SEM (n = 3) and analyzed by one-way ANOVA with post hoc test (Tukey) (F–J). **p < 0.01, ***p < 0.001, ****p < 0.0001. Scale bar, 100 μm.

See also Figure S1.

was detected in the supernatant in the presence of ATP. Resuspension of microsomes in 50% reticulocyte lysate plus ATP also resulted in a time-dependent appearance of GB_{1e} in the supernatant (Figure 2E). These data demonstrate the export of GB_{1e} in this cell-free system.

Finally, we showed that the treatment of MDA-MB-231 and MCF7-GB_{1e} cells with MG132, a proteasomal inhibitor, increased GB_{1e} levels in the TCLs (Figure 2F). The effect was observed at 6 hours posttreatment with a maximum amount of GB_{1e} after 18 h, whereas GB_{1e} levels in the CMs were not influenced by MG132. Altogether, our results demonstrate that GB_{1e} is retrotranslocated from the ER lumen to the cytosol, where it undergoes proteasomal degradation.

GB_{1e} promotes the malignancy of human BrCa cells *in vitro*

To investigate the function of GB_{1e} in BrCa cells, GB_{1e} was overexpressed in the poorly tumorigenic MCF7 and T-47D cells. Conversely, endogenous GB_{1e} was silenced in the highly tumorigenic MDA-MB-231 and BT-549 cells by using two different shRNAs (sh-GB_1 #1 and sh-GB_1 #2) targeting two different regions of the GB_1 mRNA (Figure S1B).

GB_{1e} overexpression accelerated the proliferation of MCF7 and T-47D cells (Figures 3A and 3B), whereas GB_{1e} silence remarkably slowed down the proliferation of MDA-MB-231 and BT-549 cells (Figures 3E and 3F). Moreover, GB_{1e} overexpression markedly increased the numbers of colonies and spheroids formed by MCF7 and T-47D cells (Figures 3C and 3D), but GB_{1e} silence significantly inhibited the clonogenicity and spheroid formation of MDA-MB-231 and BT-549 cells (Figures 3G and 3H). Furthermore, the numbers of migrated and invaded MDA-MB-231 and BT-549 cells were dramatically decreased by silenced GB_{1e} (Figures 3I and 3J). These results demonstrate that GB_{1e} has a tumorigenic role in BrCa cells.

GB_{1e} silence suppresses the growth and metastasis of BrCa cells in nude mice

GB_{1e} silenced or control MDA-MB-231 cells were subcutaneously injected into the dorsal flanks of athymic BALB/c mice. The tumors induced by GB_{1e} silenced cells showed longer latency and smaller mean volume than those induced by control cells (Figures 4A and 4B). Correspondingly, the average tumor weights were dramatically reduced by GB_{1e} silence (Figure 4C). In tumor xenografts induced by GB_{1e} silenced cells, GB_{1e} expression was barely detectable, and the percentage of Ki-67 positive cells was significantly decreased compared with that in the control tumors (Figure 4D). It suggested that GB_{1e} promotes the growth of BrCa cells *in vivo*.

When GB_{1e} silenced MDA-MB-231 cells were injected into the tail vein of athymic BALB/c mice, the lung metastasis was suppressed compared with the control MDA-MB-231 cells (Figures 4E and 4F). Large tumor cell mass was detected in the lungs of mice injected with control cells, but GB_{1e} silence markedly inhibited the colonization of MDA-MB-231 cells in the lungs (Figure 4G). These results suggest that GB_{1e} promotes the metastasis induced by MDA-MB-231 cells.

GB_{1e} displaces EGFR-bound PTPN12 and enhances EGFR activity

The *in vivo* data indicate that GB_{1e} is oncogenic. To investigate the oncogenic mechanism of GB_{1e}, GB_{1e} interacting proteins in MCF7-GB_{1e} cells were analyzed by tandem LC/MS/MS, and PTPN12 appeared to be one of the candidate proteins (Table S1). Co-immunoprecipitation (co-IP) analysis revealed that Flag-GB_{1e} and PTPN12 are in the same complex in MCF7 and T-47D cells transfected with either Flag-GB_{1e} or the

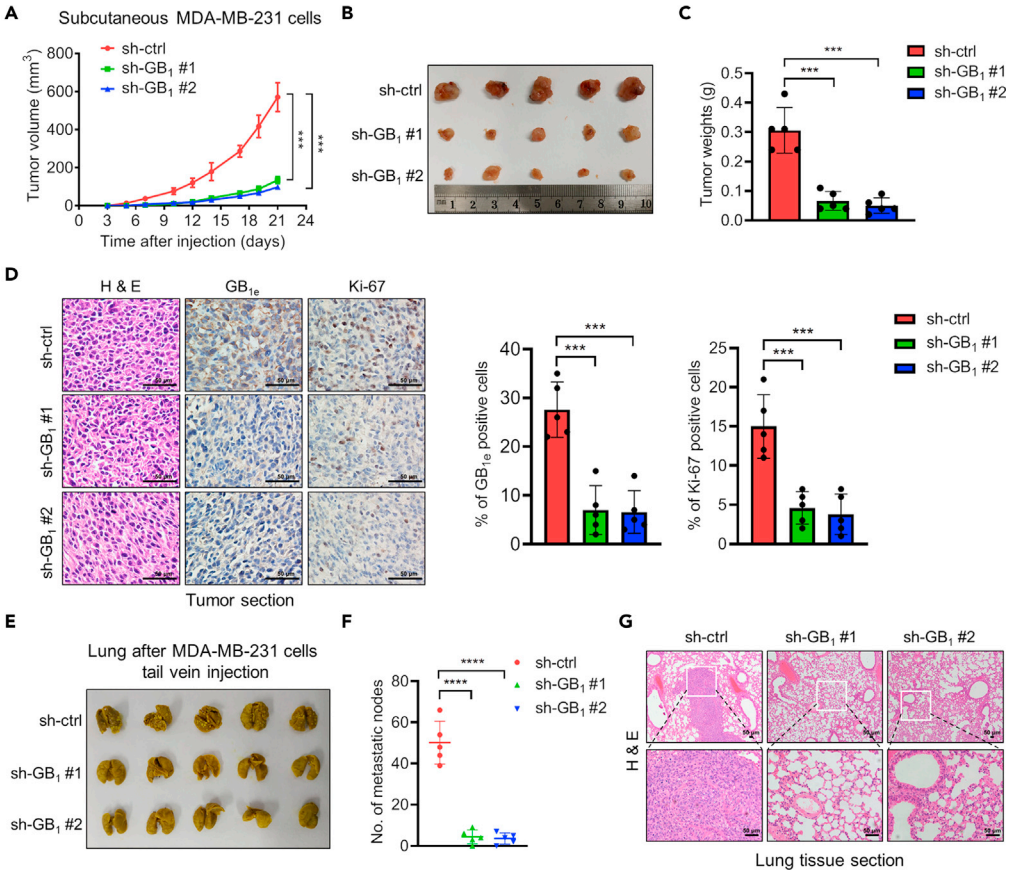

Figure 4. GB_{1e} silencing suppresses the growth and metastasis of MDA-MB-231 cells in nude mice

(A–D) 1×10^6 MDA-MB-231 cells stably transfected with sh-GB_1 #1, #2, or sh-ctrl (control shRNA) were subcutaneously injected into the dorsal flanks of BALB/c nude mice (n = 5). (A) Growth curves of tumor xenografts induced by GB_{1e} silenced versus control cells. (B) Images of tumor xenografts harvested 21 days after cell injection. (C) Weights of tumor. (D) Representative images of tumor paraffin sections stained with hematoxylin and eosin (H&E) or subjected to IHC analysis with antibodies against GB_1 and Ki-67 (cell proliferation marker). The histograms indicated the percentage of GB_1 or Ki-67 positive cells. Data are shown as mean ± SEM (n = 5) and analyzed by one-way ANOVA with post hoc test (Tukey). ***$p < 0.001$. Scale bar, 50 μm.

(E–G) GB_{1e} silenced or control MDA-MB-231 cells (2×10^5) were injected into the tail veins of BALB/c nude mice. Two weeks later, the mice were sacrificed and lungs were isolated. (E) Images of lungs fixed with Bouin solution. (F) Scatter plot indicating the number of visible metastatic nodules in the lungs. (G) Representative images of tissue sections stained with H&E. Data are shown as mean ± SEM (n = 5) and analyzed by one-way ANOVA with post hoc test (Tukey). ****$p < 0.0001$. Scale bar, 50 μm.

See also Figure S6.

empty vector (Figure 5A). Similar results were obtained in the reciprocal co-IP experiment (Figure 5B). These results suggest that both endogenous and overexpressing GB_{1e} interact with PTPN12. Of note, a pair of sushi domains (SDs) is located at the N-terminus of GB_{1e} (Figure S5A). SDs have been reported to mediate protein-protein interactions (Lehtinen et al., 2004; Terunuma, 2018). Interestingly, similar co-IP results were obtained with GB_{1e} truncated with SD sequence (Figures S5B and S5C), indicating that the interaction between GB_{1e} and PTPN12 is independent of GB_{1e} SDs.

It was demonstrated that PTPN12 can dephosphorylate EGFR (Li et al., 2015; Nair et al., 2018; Sun et al., 2011). Co-IP experiments showed that the endogenous PTPN12 and EGFR are in the same complexes in MCF7 and T-47D cells stably transfected with GB_{1e} as well as in GB_{1e} silenced MDA-MB-231 and BT-549 cells (Figures 5C and 5D). Interestingly, the association between PTPN12 and EGFR was reduced in GB_{1e} transfected cells (Figure 5C) but enhanced in GB_{1e} silenced cells (Figure 5D). These results are consistent with a model that GB_{1e} is a competitor for the interaction between PTPN2 and EGFR and these three

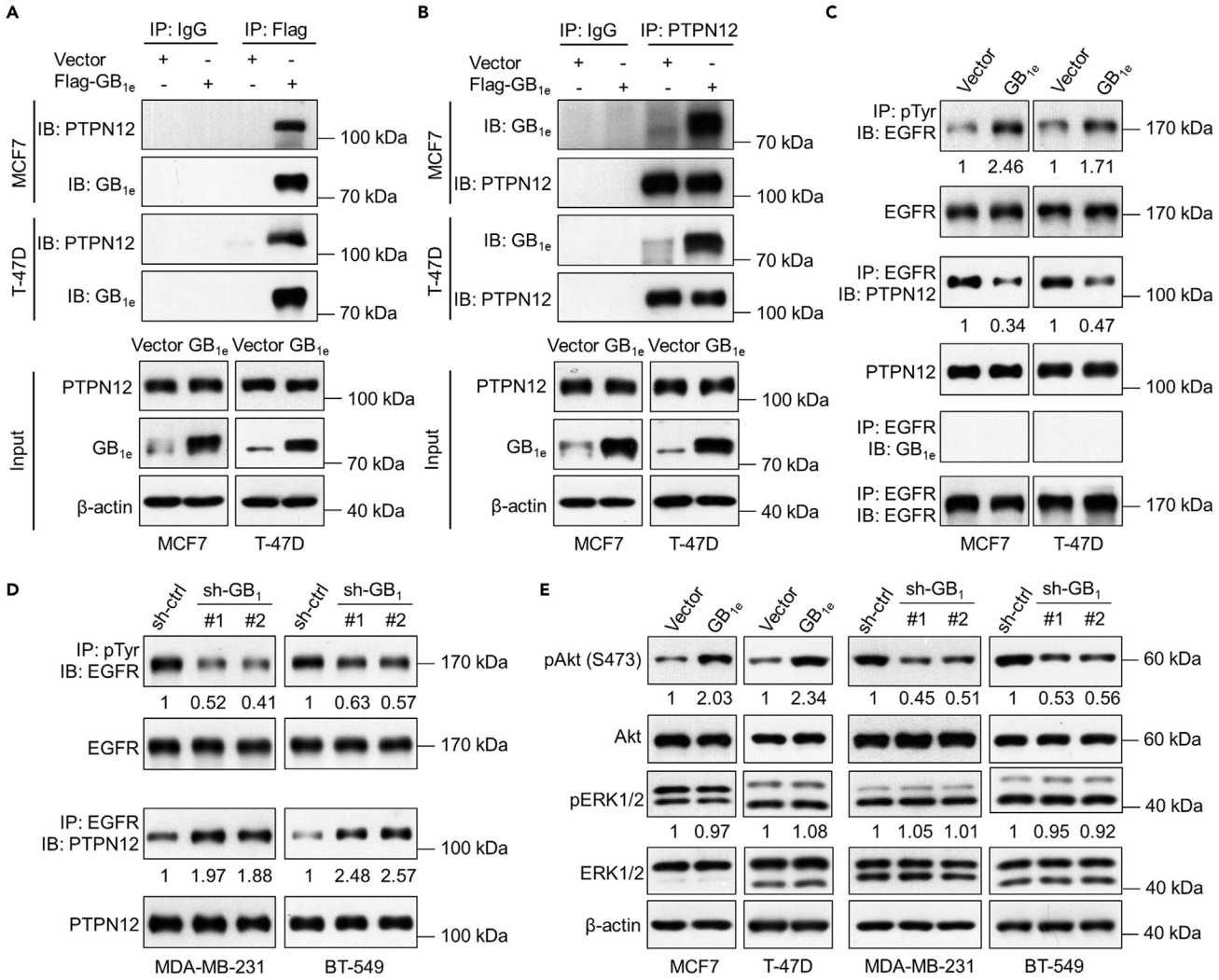

Figure 5. GB_{1e} displaces EGFR-bound PTPN12 and enhances EGFR activity

(A–C) TCLs from MCF7 and T-47D cells stably transfected with GB_{1e} or vector were subjected to co-IP and/or IP analysis. (A–B) (Upper panels) The TCLs were immunoprecipitated with anti-Flag (A) or anti-PTPN12 (B) antibody, and the immunoprecipitates were probed with anti-PTPN12 and anti-GB_1 antibodies. Mouse IgG was used as a negative control. (Lower panels) Immunoblot analysis assessing the levels of PTPN12, GB_{1e}, and β-actin in the input. (C) TCLs were immunoprecipitated with 4G10 or anti-EGFR antibody; the precipitates were probed with anti-EGFR, anti-PTPN12, or anti-GB_1 antibody. The input levels of EGFR and PTPN12 were evaluated by immunoblotting. The intensity of each immunoblot band was quantitated by ImageJ, and the data were presented as the fold changes (mean ± SEM; n = 3).

(D) TCLs from MDA-MB-231 and BT-549 cells transfected with sh-GB_1 #1, #2, or sh-ctrl (control shRNA) were immunoprecipitated with 4G10 or anti-EGFR antibody, and the precipitates were probed with anti-EGFR and anti-PTPN12 antibodies. The input levels of EGFR and PTPN12 were analyzed by immunoblotting. The intensity of each immunoblot band was quantitated by ImageJ, and the data were presented as the fold changes (mean ± SEM; n = 3).

(E) Immunoblot analysis assessing the levels of pAkt (S473), total Akt, pERK1/2, and total ERK1/2 in the indicated cells. β-actin was used as a loading control. The intensity of each immunoblot band was quantitated by ImageJ, and the data were presented as the fold changes (mean ± SEM; n = 3).

See also Figures S5, S6, S7, S8 and Table S1.

proteins cannot be in the same complex, which is in agreement with the absence of co-IP between GB_{1e} and EGFR (Figure 5C).

To examine the effect of GB_{1e} on EGFR activity, co-IP was performed using the anti-phosphotyrosine antibody 4G10 and immunoblotted with an anti-EGFR antibody. The results revealed that overexpression of GB_{1e} dramatically increased EGFR phosphorylation in MCF7 and T-47D cells (Figure 5C), but GB_{1e} silence significantly reduced EGFR phosphorylation in MDA-MB-231 and BT-549 cells (Figure 5D). These data suggested that GB_{1e} limits the negative effect of PTPN12 on EGFR activity.

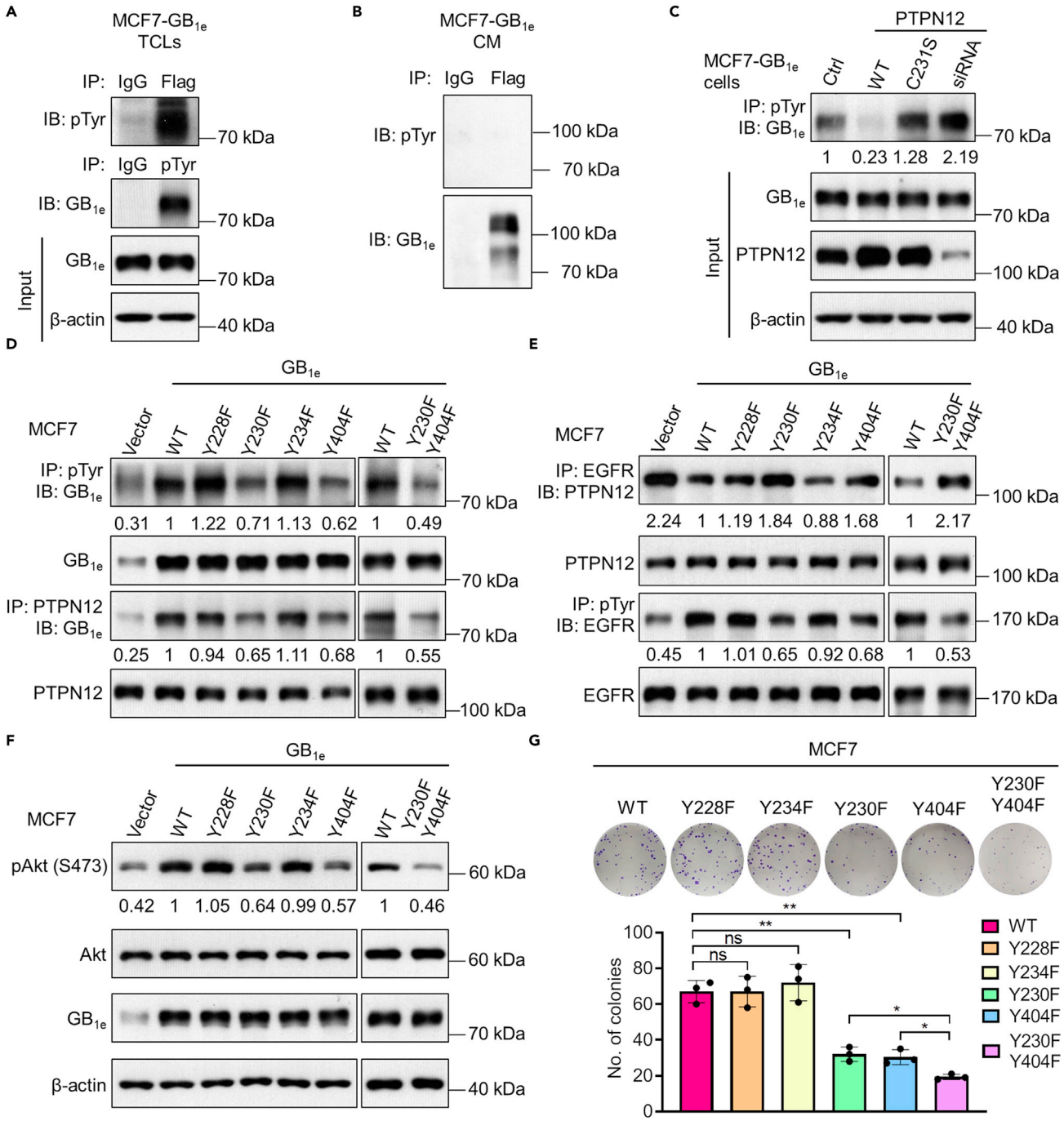

Figure 6. Phosphorylation of Y230 and Y404 on GB_{1e} is critical for GB_{1e} to hijack PTPN12 from EGFR

(A and B) TCLs (A) and CM (B) from MCF7-GB_{1e} cells were immunoprecipitated with 4G10 (A) or anti-Flag (A and B) antibody, and the precipitates were probed with anti-GB_1 or 4G10 antibody. The levels of GB_{1e} and β-actin in the input (A) were evaluated by immunoblotting.

(C) TCLs from MCF7-GB_{1e} cells transfected with wild-type (WT) PTPN12, catalytic dead PTPN12 (C231S), or PTPN12 siRNA were immunoprecipitation with 4G10 antibody, and the precipitates were probed with anti-GB_1 antibody. The input levels of GB_{1e}, PTPN12, and β-actin were evaluated by immunoblotting. The intensity of each immunoblot band was quantitated by ImageJ, and the data were expressed as the fold changes (mean ± SEM; n = 3).

(D) TCLs from MCF7 cells transfected with the indicated constructs were immunoprecipitated with 4G10 or anti-PTPN12 antibody, and the precipitates were subjected to immunoblotting with anti-GB_1 antibody. The input levels of GB_{1e} and PTPN12 were evaluated by immunoblot assay. The intensity of each immunoblot band was quantitated by ImageJ, and the data were expressed as the fold changes (mean ± SEM; n = 3).

Figure 6. *Continued*

(E) TCLs from MCF7 cells transfected with the indicated constructs were immunoprecipitated with anti-EGFR or 4G10 antibody, and the precipitates were probed with antibody against PTPN12 or EGFR. The input levels of PTPN12 and EGFR were assessed by immunoblotting. The intensity of each immunoblot band was quantitated by ImageJ, and the data were expressed as the fold changes (mean ± SEM; n = 3).

(F) Immunoblot analysis of pAkt (S473), total Akt, and GB_{1e} levels in MCF7 cells transfected with the indicated constructs. β-actin was used as a loading control. The intensity of each immunoblot band was quantitated by ImageJ, and the data were expressed as the fold changes (mean ± SEM; n = 3).

(G) Clonogenic assay of MCF7 cells transfected with the indicated constructs. The representative images and the number of colonies were shown. The data are presented as mean ± SEM (n = 3) and analyzed by one-way ANOVA with post hoc test (Tukey). ns, not significant, *p < 0.05, **p < 0.01.

See also Figures S1, S9 and S10.

We then analyzed the effects of GB_{1e} on EGFR downstream signaling. GB_{1e} overexpression significantly increased the level of Akt phosphorylation in MCF7 and T-47D cells, whereas GB_{1e} silencing in MDA-MB-231 and BT-549 cells reduced Akt phosphorylation (Figure 5E). It was also the case in tumor xenografts induced by GB_{1e} silenced MDA-MB-231 cells where Akt phosphorylation was markedly reduced (Figure S6A). This effect was specific for Akt signaling because neither overexpression nor silence of GB_{1e} altered the activities of ERK1/2 and STAT3 (Figures 5E and S6B). Akt phosphorylation was abrogated by Tarceva (erlotinib), a small molecule inhibitor of EGFR (Sharma et al., 2007), suggesting that Akt activation was downstream of EGFR (Figure S6C). We also bring results to show that the effects of GB_1 shRNA on BrCa cells resulted from GB_{1e} silence. GB_{1e} silencing was rescued by transfecting GB_{1e} silenced MDA-MB-231 cells with GB_{1e} cDNA (Figure S7A) that significantly decreased the interaction between EGFR and PTPN12 (Figure S7B) but increased the phosphorylation of EGFR and Akt (Figures S7B and S7C). Moreover, GB_{1e} rescue markedly increased the clonogenicity and migration capacity of GB_{1e} silenced cells (Figures S7D and S7E). Altogether, these results suggested that GB_{1e} induced a biased EGFR signaling by activating Akt specifically.

Finally, we showed that oncogenic effects of GB_{1e} are not influenced by $GABA_B$ receptor agonist and antagonist. Indeed, although GB_{1e} contains the same ECD as GB_{1a}, neither baclofen nor the competitive antagonist CGP54626 had effects on cell proliferation, Akt phosphorylation, and colony formation (Figure S8).

Phosphorylation of Y230 and Y404 on GB_{1e} is critical for GB_{1e} to hijack PTPN12 from EGFR

We provided evidence that the phosphorylation state of GB_{1e} is modulated by PTPN12, which has been reported to recognize specific phosphotyrosine residues on its substrates (Li et al., 2016). Tyrosine phosphorylated GB_{1e} was detected in the TCLs from MCF7-GB_{1e} cells but not in the CM (Figures 6A and 6B). The phosphorylation level of GB_{1e} was dramatically reduced by transfected WT PTPN12, but increased by PTPN12 siRNA, while not significantly altered by the PTPN12 C231S mutant that had a dead catalytic site (Figure 6C).

To identify the phosphorylation sites on GB_{1e}, we first performed a bioinformatics analysis. The potential phosphorylation sites, Y228, Y230, Y234, and Y404, were mutated to phenylalanine. The Y230F and Y404F mutations significantly reduced GB_{1e} phosphorylation in MCF7 cells, whereas the expression level of each GB_{1e} mutant was comparable with that of WT GB_{1e} (Figure 6D). When both Y230 and Y404 were mutated, GB_{1e} phosphorylation was further reduced (Figures 6D and S9A). Y230 and Y404 are therefore the main phosphorylation sites on GB_{1e}.

We also showed that phosphorylation of Y230 and Y404 on GB_{1e} is essential for GB_{1e} to interact with PTPN12, to enhance EGFR-dependent Akt signaling, and for its oncogenic effects. Compared with WT GB_{1e}, the mutants Y230F and Y404F and the double mutant dramatically decreased the co-IP between PTPN12 and GB_{1e} (Figures 6D and S9B) but enhanced the co-IP between PTPN12 and EGFR (Figures 6E and S9C). These mutants also significantly reduced the phosphorylation levels of EGFR (Figures 6E and S9D) and Akt (Figures 6F and S9E). In contrast, the mutants Y228F and Y234F had a similar effect as the WT GB_{1e} on these co-IP experiments (Figure 6D) and on the phosphorylation of EGFR (Figure 6E) and Akt (Figure 6F). Finally, the mutants Y230F and Y404F and the double mutant markedly decreased the colony numbers formed by MCF7 cells, but the Y228F and Y234F mutations on GB_{1e} did not (Figure 6G). Altogether, these results suggested that the oncogenic effects of GB_{1e} are mainly dependent on the phosphorylation of Y230 and Y404.

DISCUSSION

In this study, we made an observation that GB_{1e} is the predominant GB_1 isoform at both mRNA and protein levels in various human BrCa cell lines and tissues. Moreover, the expression level of GB_{1e} correlates with

the tumorigenic potential of BrCa cell lines and is upregulated in BrCa tissues. Interestingly, ER^+/PR^+, $Her2^+$, and triple negative cell lines displayed low, medium, and high expression levels of GB_{1e}, respectively, suggesting that GB_{1e} expression correlates with the expression of ER, PR, and Her2 in breast cancer cells. GB_{1e} not only enhances the proliferation, migration, and invasion of human BrCa cells *in vitro* but also promotes the growth and metastasis of BrCa cells *in vivo*. Furthermore, GB_{1e} enhances EGFR signaling by displacing EGFR-bound PTPN12. Our results suggest an original mode of action of GB_{1e} involved in the development and progression of human BrCa.

Although GB_{1e} has a N-terminal signal peptide and it can be secreted as the other GB_{1a} isoforms, our results showed an original mechanism of GB_{1e} action. It is different from what have been reported previously that $GABA_B$ receptor induced EGFR transactivation in a $G_{i/o}$ protein dependent way (Xia et al., 2017). It also differs from the previous study that has shown the membrane-associated GB_{1e} can form heterodimer with GB_2 and disrupt the normal association between GB_{1a} and GB_2 but have no effect on $GABA_B$ receptor activation (Schwarz et al., 2000). Our data suggested that GB_{1e} is retrotranslocated from the ER lumen to the cytosol. ER is the major site of protein synthesis and processing, and misfolded/unfolded proteins are identified and removed by a process called ER-associated degradation (ERAD), in which the proteins are transported to the cytosol and degraded by proteasomes (Oikonomou and Hendershot, 2020). However, the ERAD system is not always coupled to protein degradation. Clusterin, a secreted glycoprotein, can interact with conformationally altered Bax and inhibit the apoptosis of cancer cells once being retrotranslocated to the cytosol under stressed conditions (Nizard et al., 2007; Zhang et al., 2005). Our results indicated that GB_{1e} might be recognized as a misfolded protein by ERAD components and then being retrotranslocated to the cytosol. It is in agreement with the observation that the isolated GB_1 ECD appears unfolded in the absence of ligand (Geng et al., 2012). It is also consistent that neither baclofen nor CGP54626 influences the proliferation and clonogenicity of MCF7-GB_{1e} cells, in agreement with that GB_{1e} ectopically expressed in HEK293 cells did not bind CGP54626 (Schwarz et al., 2000).

Our results suggest that GB_{1e} interacts with PTPN12 in the cytosol and then prevents this phosphatase to dephosphorylate EGFR and enhances Akt signaling, a pathway that could be responsible for the oncogenic role of GB_{1e}. More than 20 substrates and binding partners of PTPN12 have been identified (Li et al., 2015; Nair et al., 2018). PTPN12 functions as a tumor suppressor in BrCa cells by dephosphorylating and inactivating EGFR, Her2, and other RTKs (Nair et al., 2018; Sun et al., 2011). Consistent with the published data, we detect an association between PTPN12 and EGFR in human BrCa cells. Our data suggest that GB_{1e} and EGFR compete for PTPN12 interaction. Of note, GB_{1e} SDs are not directly involved in this process, in contrast to the N-terminal SDs of GB_{1a} that have been shown to interact with amyloid-β precursor protein, adherence-junction associated protein 1, PILRα-associated neural protein, and extracellular matrix protein fibulin-2 for axonal trafficking and synaptic transmission (Blein et al., 2004; Dinamarca et al., 2019; Rice et al., 2019).

Interestingly, the association between GB_{1e} and PTPN12 is dependent on tyrosine phosphorylation of GB_{1e}. Phosphorylation plays a key role in regulating protein function, and an estimated 30% of cellular proteins undergo phosphorylation (Qiu et al., 2020). Although the activity of $GABA_B$ receptor is not correlated with its overall phosphorylation state, the surface stability, endocytosis, and desensitization of $GABA_B$ receptor are regulated by phosphorylation of several serine residues in the intracellular regions of GB_1 (S867, S917, and S923) and GB_2 (Guetg et al., 2010; Kuramoto et al., 2007; Pontier et al., 2006; Rose and Wickman, 2020). Phosphorylation of the $GABA_B$ ECD and tyrosine phosphorylation of $GABA_B$ receptor has not been reported yet. We find that phosphorylation of GB_{1e} at multiple tyrosine sites, especially Y230 and Y404, plays a key role in disrupting EGFR-PTPN12 interaction and upregulating EGFR-Akt signaling cascade. Of note, Y230 and Y404 are located on two different lobes of the GB_1 ECD (Figure S10A), but they are on two close faces that are nearby the interface between GB_1 and GB_2 ECD in the $GABA_B$ receptor. In addition, although Y230 is highly conserved during evolution, Y404 is conserved only in mammals (Figure S10B). Finally, the kinases that phosphorylate GB_{1e} need to be further identified.

In addition to human breast cancer cells, GB_{1e} expression was also detected in human prostate cancer cell lines (LNCaP, PC-3, and DU145) and tissues; moreover, four out of five human prostate cancer specimens showed increased protein expression of GB_{1e} compared with matched tumor adjacent tissues (Figures S11A–S11C). Therefore, dysregulated GB_{1e} expression may occur in various human cancers and is not specific to breast cancer. Moreover, the other human cancer cell lines including glioma (U251 and U87), hepatocarcinoma (BEL7402, HEPG2, HCCLM9), and colon cancer (CACO2, SW480) cell lines also showed GB_{1e}

expression with variable levels (Figures S11A and S11B). Interestingly, GB_{1e} protein level in the two glioma cell lines is lower than those in the other cancer cell lines. Because heterodimeric $GABA_B$ receptors are predominantly expressed in the central nervous system, whereas GB_{1e} is the main GB_1 isoform in the peripheral tissues, we assume that heterodimeric $GABA_B$ receptors and GB_{1e} may play essential roles in the development and progress of brain tumor and nonneural-tissue-derived tumors, respectively.

Taken together, this study demonstrates that GB_{1e} is a tumorigenic protein in BrCa cells and promotes the malignancy of BrCa cells both *in vitro* and *in vivo*. Cytosolic GB_{1e} may undergo tyrosine phosphorylation or proteasomal degradation. Phosphorylation of Y230 and Y404 on GB_{1e} is critical for GB_{1e} to displace EGFR-bound PTPN12 and activate EGFR-Akt signaling pathway. This study, therefore, provides a new strategy for the treatment of BrCa by targeting the interactions between GB_{1e}, PTPN12, and EGFR.

Limitations of the study

Although our *in vitro* and *in vivo* study clearly demonstrates that GB_{1e} has a tumorigenic function in breast cancer cells and always is upregulated in breast cancer tissues, its exploitation in clinical value needed to be further studied. In addition, we did not analyze the function of the secreted GB_{1e}. It is meaningful to further investigate whether secreted GB_{1e} can promote breast cancer progression by regulating tumor microenvironment. In addition, it is also valuable to evaluate whether secreted GB_{1e} is a potential marker for clinical diagnosis.

STAR★METHODS

Detailed methods are provided in the online version of this paper and include the following:

- KEY RESOURCES TABLE
- RESOURCE AVAILABILITY
  - Lead contact
  - Materials availability
  - Data and code availability
- EXPERIMENTAL MODEL AND SUBJECT DETAILS
  - Cell lines
  - Tumor xenografts and experimental metastasis
- METHOD DETAILS
  - Human BrCa specimens
  - Plasmid construction
  - Cell transfection
  - Reverse transcriptase and real time PCR
  - Proliferation, colony and spheroid formation
  - Transwell assay
  - Enzyme linked immunosorbent assay (ELISA)
  - Immunoprecipitation
  - Immunoblotting
  - Immunofluorescence
  - LC-MS/MS analysis
  - Immunohistochemistry
  - Microsome isolation
  - Protease protection assays
  - Protein export assay
  - Treat cells with $GABA_B$ receptor agonist
- QUANTIFICATION AND STATISTICAL ANALYSIS

SUPPLEMENTAL INFORMATION

Supplemental information can be found online at https://doi.org/10.1016/j.isci.2021.103311.

ACKNOWLEDGMENTS

This study was supported by the grants from the Ministry of Science and Technology of China (Grant 2018YFA0507003), the National Natural Science Foundation of China (Grants 31420103909, 81720108031,

31721002, and 81872945), and the Program for Introducing Talents of Discipline to the Universities of the Ministry of Education (Grant B08029). J.-P. P. and P.R. were supported by the Centre National de la Recherche Scientifique (CNRS; PRC n°1403), the Institut National de la Santé et de la Recherche Médicale (INSERM; International Research Program « Brain Signal »), and the Program Hubert Curien (PHC) Cai Yuanpei from the Ministère Français des Affaires Etrangères.

AUTHOR CONTRIBUTIONS

Conceptualization, X.J. and J.L.; Investigation, X.J., J.L., B.W., Y.Z., S.W., X.W., S.X., X.S., and Z.Z.; Methodology, X.J. and B.W.; Software, S.W.; Resources, P.Y. and Y.H.; Writing—Original Draft, X.J., B.W., J.L., P.R., and P.P.; Writing—Review & Editing, X.J., B.W., and P.R.; Funding Acquisition, J.L., P.R., and P.P.; Supervision, X.J. and J.L. All authors have read and agreed to the revised version of the manuscript.

DECLARATION OF INTERESTS

The authors declare no competing interests.

Received: August 11, 2021
Revised: September 24, 2021
Accepted: October 14, 2021
Published: November 19, 2021

REFERENCES

Azuma, H., Inamoto, T., Sakamoto, T., Kiyama, S., Ubai, T., Shinohara, Y., Maemura, K., Tsuji, M., Segawa, N., Masuda, H., et al. (2003). Gamma-aminobutyric acid as a promoting factor of cancer metastasis; induction of matrix metalloproteinase production is potentially its underlying mechanism. Cancer Res. *63*, 8090–8096.

Bettler, B., Kaupmann, K., Mosbacher, J., and Gassmann, M. (2004). Molecular structure and physiological functions of $GABA_B$ receptors. Physiol. Rev. *84*, 835–867.

Blein, S., Ginham, R., Uhrin, D., Smith, B.O., Soares, D.C., Veltel, S., McIlhinney, R.A., White, J.H., and Barlow, P.N. (2004). Structural analysis of the complement control protein (CCP) modules of $GABA_B$ receptor 1a: only one of the two CCP modules is compactly folded. J. Biol. Chem. *279*, 48292–48306.

Dinamarca, M.C., Raveh, A., Schneider, A., Fritzius, T., Früh, S., Rem, P.D., Stawarski, M., Lalanne, T., Turecek, R., Choo, M., et al. (2019). Complex formation of APP with $GABA_B$ receptors links axonal trafficking to amyloidogenic processing. Nat. Commun. *10*, 1331.

Fava, G., Marucci, L., Glaser, S., Francis, H., De Morrow, S., Benedetti, A., Alvaro, D., Venter, J., Meininger, C., Patel, T., et al. (2005). gamma-Aminobutyric acid inhibits cholangiocarcinoma growth by cyclic AMP-dependent regulation of the protein kinase A/extracellular signal-regulated kinase 1/2 pathway. Cancer Res. *65*, 11437–11446.

Gassmann, M., and Bettler, B. (2012). Regulation of neuronal $GABA_B$ receptor functions by subunit composition. Nat. Rev. Neurosci. *13*, 380–394.

Geng, Y., Xiong, D., Mosyak, L., Malito, D.L., Kniazeff, J., Chen, Y., Burmakina, S., Quick, M., Bush, M., Javitch, J.A., et al. (2012). Structure and functional interaction of the extracellular domain of human $GABA_B$ receptor GBR2. Nat. Neurosci. *15*, 970–978.

Guetg, N., Abdel Aziz, S., Holbro, N., Turecek, R., Rose, T., Seddik, R., Gassmann, M., Moes, S., Jenoe, P., Oertner, T.G., et al. (2010). NMDA receptor-dependent $GABA_B$ receptor internalization via CaMKII phosphorylation of serine 867 in $GABA_{B1}$. Proc. Natl. Acad. Sci. U S A *107*, 13924–13929.

Huang, Q., Zhu, C.L., Liu, C.H., Xie, F., Zhu, K., and Hu, S.Y. (2013). Gamma-aminobutyric acid binds to $GABA_B$ receptor to inhibit cholangiocarcinoma cells growth via the JAK/STAT3 pathway. Dig. Dis. Sci. *58*, 734–743.

Inamoto, T., Azuma, H., Sakamoto, T., Kiyama, S., Ubai, T., Kotake, Y., Watanabe, M., and Katsuoka, Y. (2007). Invasive ability of human renal cell carcinoma cell line Caki-2 is accelerated by gamma-aminobutyric acid, via sustained activation of ERK1/2 inducible matrix metalloproteinases. Cancer Invest. *25*, 574–583.

Jiang, X., Su, L., Zhang, Q., He, C., Zhang, Z., Yi, P., and Liu, J. (2012). $GABA_B$ receptor complex as a potential target for tumor therapy. J. Histochem. Cytochem. *60*, 269–279.

Joseph, J., Niggemann, B., Zaenker, K.S., and Entschladen, F. (2002). The neurotransmitter gamma-aminobutyric acid is an inhibitory regulator for the migration of SW 480 colon carcinoma cells. Cancer Res. *62*, 6467–6469.

Kuramoto, N., Wilkins, M.E., Fairfax, B.P., Revilla-Sanchez, R., Terunuma, M., Tamaki, K., Iemata, M., Warren, N., Couve, A., Calver, A., et al. (2007). Phospho-dependent functional modulation of $GABA_B$ receptors by the metabolic sensor AMP-dependent protein kinase. Neuron *53*, 233–247.

Lehtinen, M.J., Meri, S., and Jokiranta, T.S. (2004). Interdomain contact regions and angles between adjacent short consensus repeat domains. J. Mol. Biol. *344*, 1385–1396.

Li, H., Yang, F., Liu, C., Xiao, P., Xu, Y., Liang, Z., Liu, C., Wang, H., Wang, W., Zheng, W., et al. (2016). Crystal structure and substrate specificity of PTPN12. Cell Rep. *15*, 1345–1358.

Li, J., Davidson, D., Martins Souza, C., Zhong, M.C., Wu, N., Park, M., Muller, W.J., and Veillette, A. (2015). Loss of PTPN12 stimulates progression of ErbB2-dependent breast cancer by enhancing cell survival, migration, and epithelial-to-mesenchymal transition. Mol. Cell. Biol. *35*, 4069–4082.

Mizuta, K., Osawa, Y., Mizuta, F., Xu, D., and Emala, C.W. (2008). Functional expression of $GABA_B$ receptors in airway epithelium. Am. J. Respir. Cell Mol. Biol. *39*, 296–304.

Nair, A., Chung, H.C., Sun, T., Tyagi, S., Dobrolecki, L.E., Dominguez-Vidana, R., Kurley, S.J., Orellana, M., Renwick, A., Henke, D.M., et al. (2018). Combinatorial inhibition of PTPN12-regulated receptors leads to a broadly effective therapeutic strategy in triple-negative breast cancer. Nat. Med. *24*, 505–511.

Neophytou, C., Boutsikos, P., and Papageorgis, P. (2018). Molecular mechanisms and emerging therapeutic targets of triple-negative breast cancer metastasis. Front. Oncol. *8*, 31.

Nizard, P., Tetley, S., Le Dréan, Y., Watrin, T., Le Goff, P., Wilson, M.R., and Michel, D. (2007). Stress-induced retrotranslocation of clusterin/ApoJ into the cytosol. Traffic *8*, 554–565.

Oikonomou, C., and Hendershot, L.M. (2020). Disposing of misfolded ER proteins: a troubled substrate's way out of the ER. Mol. Cell Endocrinol. *500*, 110630.

Pin, J.P., and Bettler, B. (2016). Organization and functions of mGlu and $GABA_B$ receptor complexes. Nature *540*, 60–68.

Pin, J.P., Kniazeff, J., Binet, V., Liu, J., Maurel, D., Galvez, T., Duthey, B., Havlickova, M., Blahos, J., Prezeau, L., et al. (2004). Activation mechanism of

the heterodimeric $GABA_B$ receptor. Biochem. Pharmacol. *68*, 1565–1572.

Pontier, S.M., Lahaie, N., Ginham, R., St-Gelais, F., Bonin, H., Bell, D.J., Flynn, H., Trudeau, L.E., McIlhinney, J., White, J.H., et al. (2006). Coordinated action of NSF and PKC regulates $GABA_B$ receptor signaling efficacy. EMBO J. *25*, 2698–2709.

Qiu, W., Evans, C.A., Landels, A., Pham, T.K., and Wright, P.C. (2020). Phosphopeptide enrichment for phosphoproteomic analysis - a tutorial and review of novel materials. Anal. Chim. Acta *1129*, 158–180.

Qu, J., Zou, T., and Lin, Z. (2021). The roles of the ubiquitin-proteasome system in the endoplasmic reticulum stress pathway. Int. J. Mol. Sci. *22*, 1526.

Rice, H.C., de Malmazet, D., Schreurs, A., Frere, S., Van Molle, I., Volkov, A.N., Creemers, E., Vertkin, I., Nys, J., Ranaivoson, F.M., et al. (2019). Secreted amyloid-β precursor protein functions as a $GABA_BR1a$ ligand to modulate synaptic transmission. Science *363*, eaao4827.

Rose, T.R., and Wickman, K. (2020). Mechanisms and regulation of neuronal $GABA_B$ receptor-dependent signaling. Curr. Top Behav. Neurosc. Published online in advance. https://doi.org/10.1007/7854_2020_129.

Schmitz, A., Herrgen, H., Winkeler, A., and Herzog, V. (2000). Cholera toxin is exported from microsomes by the Sec61p complex. J. Cell Biol. *148*, 1203–1212.

Schuller, H.M. (2008). Neurotransmission and cancer: implications for prevention and therapy. Anti-Cancer Drugs *19*, 655–671.

Schwarz, D.A., Barry, G., Eliasof, S.D., Petroski, R.E., Conlon, P.J., and Maki, R.A. (2000). Characterization of gamma-aminobutyric acid receptor $GABA_{B(1e)}$, a $GABA_{B(1)}$ splice variant encoding a truncated receptor. J. Biol. Chem. *275*, 32174–32181.

Sharma, S.V., Bell, D.W., Settleman, J., and Haber, D.A. (2007). Epidermal growth factor receptor mutations in lung cancer. Nat. Rev. Cancer *7*, 169–181.

Sun, T., Aceto, N., Meerbrey, K.L., Kessler, J.D., Zhou, C., Migliaccio, I., Nguyen, D.X., Pavlova, N.N., Botero, M., Huang, J., et al. (2011). Activation of multiple proto-oncogenic tyrosine kinases in breast cancer via loss of the PTPN12 phosphatase. Cell *144*, 703–718.

Sung, H., Ferlay, J., Siegel, R.L., Laversanne, M., Soerjomataram, I., Jemal, A., and Bray, F. (2021). Global cancer statistics 2020: GLOBOCAN estimates of incidence and mortality worldwide for 36 cancers in 185 countries. CA. Cancer J. Clin. *71*, 209–249.

Tatsuta, M., Iishi, H., Baba, M., Nakaizumi, A., Ichii, M., and Taniguchi, H. (1990). Inhibition by gamma-amino-n-butyric acid and baclofen of gastric carcinogenesis induced by N-methyl-N'-nitro-N-nitrosoguanidine in Wistar rats. Cancer Res. *50*, 4931–4934.

Terunuma, M. (2018). Diversity of structure and function of $GABA_B$ receptors: a complexity of $GABA_B$-mediated signaling. Proc. Jpn. Acad. Ser. B. Phys. Biol. Sci. *94*, 390–411.

Thaker, P.H., Yokoi, K., Jennings, N.B., Li, Y., Rebhun, R.B., Rousseau, D.L., Jr., Fan, D., and Sood, A.K. (2005). Inhibition of experimental colon cancer metastasis by the GABA-receptor agonist nembutal. Cancer Biol. Ther. *4*, 753–758.

Wahlman, J., DeMartino, G.N., Skach, W.R., Bulleid, N.J., Brodsky, J.L., and Johnson, A.E. (2007). Real-time fluorescence detection of ERAD substrate retrotranslocation in a mammalian *in vitro* system. Cell *129*, 943–955.

Wang, T., Huang, W., and Chen, F. (2008). Baclofen, a $GABA_B$ receptor agonist, inhibits human hepatocellular carcinoma cell growth *in vitro* and *in vivo*. Life Sci. *82*, 536–541.

Xia, S., He, C., Zhu, Y., Wang, S., Li, H., Zhang, Z., Jiang, X., and Liu, J. (2017). $GABA_BR$- induced EGFR transactivation promotes migration of human prostate cancer cells. Mol. Pharmacol. *92*, 265–277.

Zhang, D., Li, X., Yao, Z., Wei, C., Ning, N., and Li, J. (2014). GABAergic signaling facilitates breast cancer metastasis by promoting ERK1/2-dependent phosphorylation. Cancer Lett. *348*, 100–108.

Zhang, H., Kim, J.K., Edwards, C.A., Xu, Z., Taichman, R., and Wang, C.Y. (2005). Clusterin inhibits apoptosis by interacting with activated Bax. Nat. Cell Biol. *7*, 909–915.

STAR★METHODS

KEY RESOURCES TABLE

REAGENT or RESOURCE	SOURCE	IDENTIFIER
Antibodies		
anti-GB_1	Abcam	Cat# ab55051; RRID: AB_941703
anti-Flag	Santa Cruz Biotechnology	Cat# sc-51590; RRID: AB_677316
anti-PTPN12	Santa Cruz Biotechnology	Cat# sc-65229; RRID: AB_632280
anti-Ki-67	Santa Cruz Biotechnology	Cat# sc-23900; RRID: AB_627859
anti-EGFR	Cell Signaling Technology	Cat# 2085; RRID: AB_1903953
anti-pAkt (Ser473)	Cell Signaling Technology	Cat# 4060; RRID: AB_2315049
anti-total Ak	Cell Signaling Technology	Cat# 9272; RRID: AB_329827
anti-pERK1/2 (T202/Y204)	Cell Signaling Technology	Cat# 4370; RRID: AB_2315112
anti-total ERK1/2	Cell Signaling Technology	Cat# 4695; RRID: AB_390779
anti-pSTAT3 (Tyr705)	Cell Signaling Technology	Cat# 9145; RRID: AB_2491009
anti-total STAT3	Cell Signaling Technology	Cat# 4904; RRID: AB_331269
anti-Calnexin	Cell Signaling Technology	Cat# 2679; RRID: AB_2228381
HRP-conjugated anti-Flag antibody	Cell Signaling Technology	Cat# 86861; RRID: AB_2800094
HRP-conjugated anti-rabbit IgG	Cell Signaling Technology	Cat# 7074; RRID: AB_2099233
HRP-conjugated anti-mouse IgG	Cell Signaling Technology	Cat# 7076; RRID: AB_330924
Alexa Fluor 488–conjugated anti-mouse IgG	Cell Signaling Technology	Cat# 4408; RRID: AB_10694704
anti-β-actin	Cell Signaling Technology	Cat# 4970; RRID: AB_2223172
Phosphotyrosine antibody, clone 4G10	Sigma-Aldrich	Cat# 05-321; RRID: AB_2891016
Biological samples		
Human breast cancer tissues	Union Hospital, Tongji Medical College, Huazhong University of Science and Technology, Wuhan, China	N/A
Chemicals, peptides, and recombinant proteins		
Tunicamycin	YEASEN, Shanghai	Cat# 60251ES03
Brefeldin A	Beyotime, Shanghai	Cat# S1536
Baclofen	R&D Systems	Cat# 0796
CGP54626	R&D Systems	Cat# 1088
Tarceva	Sigma-Aldrich	Cat# 183319-69-9
B-27 supplement (50x) serum free	ThermoFisher Scientific	Cat# 17504044
Human EGF Recombinant Protein	ThermoFisher Scientific	Cat# PHG0311
Human bFGF Recombinant Protein	ThermoFisher Scientific	Cat# PHG0261
BD matrigel matrix growth factor reduced	BD Biosciences	Cat# 365234
Critical commercial assays		
PrimeScript RT reagent kit	Takara	Cat# RR047A
SYBR Green PCR master mix	Applied Biosystems	Cat# 4309155
QuikChange mutagenesis kit	Agilent Technologies	Cat# 200521
Microsome isolation kit	Biovision	Cat# K249-50
Lipofectamine™ 2000 Transfection Reagent	Invitrogen	Cat# 11668019
PepMute™ siRNA Transfection Reagent	SignaGen Laboratories	Cat# SL100566

(*Continued on next page*)

Continued

REAGENT or RESOURCE	SOURCE	IDENTIFIER
Experimental models: cell lines		
MCF7	American Type Culture Collection (ATCC)	Cat# HTB-22; RRID: CVCL_0031
T-47D	American Type Culture Collection (ATCC)	Cat# HTB-133; RRID: CVCL_0553
BT-474	American Type Culture Collection (ATCC)	Cat# HTB-20; RRID: CVCL_0179
AU-565	American Type Culture Collection (ATCC)	Cat# CRL-2351; RRID: CVCL_1074
SK-BR-3	American Type Culture Collection (ATCC)	Cat# HTB-30; RRID: CVCL_0033
MDA-MB-453	American Type Culture Collection (ATCC)	Cat# HTB-131; RRID: CVCL_0418
MDA-MB-231	American Type Culture Collection (ATCC)	Cat# HTB-26; RRID: CVCL_0062
BT-549	American Type Culture Collection (ATCC)	Cat# HTB-122; RRID: CVCL_1092
MCF10A	American Type Culture Collection (ATCC)	Cat# CRL-10317; RRID: CVCL_0598
HEK293T	American Type Culture Collection (ATCC)	Cat# CRL-11268; RRID: CVCL_1926
Cerebellar granule neurons	This paper	N/A
Experimental models: organisms/strains		
Balb/c nude mice	Beijing Vital River Laboratory	N/A
Oligonucleotides		
See Table S2 for shRNA sequences of GB_1	This paper	N/A
See Table S3 for primers used for site-directed mutagenesis of GB_{1e} and PTPN12	This paper	N/A
See Table S4 for siRNA sequences of GB_1 and PTPN12	This paper	N/A
See Table S5 for RT-PCR primers of $GB_{1a/1e}$ and β-actin	This paper	N/A
See Table S6 for qRT-PCR primers of GB_{1e} and β-actin	This paper	N/A
Recombinant DNA		
pEGFP-N1-GB_{1e}	This paper	N/A
pCDNA5/FRT-PTPN12	This paper	N/A
Software and algorithms		
Graphpad Prism 8	GraphPad Software, Inc	N/A
ImageJ	ImageJ, NIH	N/A
Other		
4G10-conjugated agarose beads	Sigma-Aldrich	Cat# 16-101
EGFR antibody–conjugated sepharose beads	Cell Signaling Technology	Cat# 8083; RRID: AB_10994874
protein A-Sepharose beads	Millipore	Cat# 16-125
protein G-Sepharose beads	Millipore	Cat# 16-266

RESOURCE AVAILABILITY

Lead contact

Further information and requests for resources and reagents should be directed to and will be fulfilled by the lead contact, Jianfeng Liu (jfliu@mail.hust.edu.cn).

Materials availability

Unique reagents generated in this study are available from the lead contact with a completed Material Transfer Agreement.

Data and code availability

Data reported in this paper will be shared by the lead contact upon request.

This paper does not report original code.

Any additional information required to reanalyze the data reported in this paper is available from the lead contact upon request.

EXPERIMENTAL MODEL AND SUBJECT DETAILS

Cell lines

Human BrCa cell lines MCF7, T-47D, BT-474, AU-565, SK-BR-3, MDA-MB-453, MDA-MB-231, BT-549, and normal human breast epithelia cell line MCF10A were obtained from American Type Culture Collection. MCF7, T-47D, AU-565 and SK-BR-3 cells were maintained in complete DMEM (supplemented with 10% FBS, 100 U/mL penicillin, and 100 μg/mL streptomycin) with high glucose. BT-474 and BT-549 cells were maintained in complete RPMI-1640 medium. MDA-MB-453 and MDA-MB-231 were cultured in complete L-15 medium. MCF10A cells were grown in special medium purchased from Procell Life Science & Technology (Wuhan, China). Cerebellar granule neurons (CGNs) were dissected from the cerebella of one-week-old female Kunming mice. All cell lines were screened regularly for mycoplasma.

Tumor xenografts and experimental metastasis

Three to four-week-old female BALB/c nude mice were randomly divided into three groups (n = 5). 1×10^6 of control or GB_{1e} silenced MDA-MB-231 cells were injected subcutaneously into the dorsal flanks of mice. Starting three days post-injection, tumor size was measured every two to three days, and tumor volume was calculated according to the formula: length×width^2×0.5. The mice were sacrificed 21 days post-injection. Tumors were harvested, weighed, and subjected to hematoxylin and eosin (H&E) staining or immunohistochemistry analysis.

For experimental metastasis experiment, 2×10^5 control or GB_{1e} silenced MDA-MB-231 cells were injected into the tail veins of female BALB/c nude mice (n = 5). Two weeks later, the mice were sacrificed and the lungs were excised. The metastatic nodules were fixed with Bouin solution (Sigma) and evaluated with H&E staining.

The protocols for animal study were approved by the Institutional Animal Care and Use Committee, TMC/HUST (approval No. 2019-S2336) in accordance with the Guide for the Care and Use of Laboratory Animals. The mice were maintained in grouped cages at a temperature of 20°C–24°C, humidity of 50%–60%, pathogen-free facility on a 12 hr light/dark cycle and fed ad liberum food and water.

METHOD DETAILS

Human BrCa specimens

Human BrCa and matched para-cancerous tissues were collected from Union Hospital, Tongji Medical College (TMC), Huazhong University of Science and Technology (HUST) in accordance with the protocol approved by the Ethics Committee of TMC/HUST (approval No. 2019-S1048). Surgically removed samples were snap-frozen in liquid nitrogen and stored at −80°C until use.

Plasmid construction

Human GB_{1e} DNA (GenBank: AF301005.1) was synthesized by Sangon Biotech (Shanghai, China) and subcloned into plasmid pEGFP-N1 with Flag tag. Human PTPN12 cDNA (GenBank: NM_002835.4) was from Addgene (Watertown, MA, USA) and subcloned into pcDNA5/FRT plasmid with HA tag. GB_1 shRNAs #1 or #2 was inserted into plasmid pLVX-shRNA2-Puro. GB_{1e} mutations (Y228F, Y230F, Y234F, Y404F, and Y230F/Y404F) and PTPN12 mutation (C231S) were made by using the QuikChange mutagenesis kit (Agilent Technologies, Santa Clara, CA, USA). The shRNA sequences and primer sequences for mutagenesis were listed in Tables S2 and S3.

GB_{1e} with the deletion of sushi domain sequence (GB_{1e} (ΔSDs)) were amplified by using pEGFP-N1-Flag-GB_{1e} as the template, and the forward and reverse primers were 5′-gatcgatatcaatcgaacgccacactca-3′ and

5′-gatcggatcctcaggttgggct-3′ respectively. For PCR amplification, 35 cycles of 95°C for 30 sec, 56°C for 1 min, and 72°C for 2 min, with a final extension at 72°C for 10 min, were performed. The PCR product was cloned into plasmid pEGFP-N1 with Flag tag and verified by DNA sequencing.

Cell transfection

Plasmids encoding wild type (WT) GB_{1e}, GB_{1e} mutants (Y228F, Y230F, Y234F, Y404F, or Y230F/Y404F), WT PTPN12, or PTPN12 mutant (C231S) were transfected into MCF7 cells and/or T-47D cells by lipofectamine™ 2000 transfection reagent (Invitrogen), empty vectors were used as controls. MCF7 and T-47D cells transfected with WT GB_{1e} were selected with G418 and to get stable cell lines.

GB_{1e} or control siRNAs were transfected into MDA-MB-231 and BT-549 cells by using pepMute™ siRNA transfection reagent (SignaGen Laboratories, Rockville, MD, USA). shRNAs were synthesized based on siRNA sequences that efficiently silenced GB_{1e} expression. Lentiviral particles containing sh-GB_1 or sh-ctrl were produced in HEK293T cells and used to infect MDA-MB-231 or BT-549 cells. Puromycin selection was performed to get stable GB_{1e} silenced cell lines. PTPN12 siRNAs were transfected into MCF7 cells by using pepMute™ siRNA transfection reagent. The siRNA sequences were listed in Tables S4.

Reverse transcriptase and real time PCR

In reverse transcriptase (RT)-PCR, Trizol reagent (Invitrogen) was used to isolate total RNA from tissue specimens or cell lines. cDNA was made by using PrimeScript RT reagent kit (Takara Inc., Dalian, P.R. China) and subjected to 40 cycles of PCR. The products were separated by 2% agarose gels and analyzed by Bio-Rad Gel Doc XR+ System. Real time (qRT)-PCR was performed by using SYBR Green PCR master mix (Applied Biosystems, Foster City, CA, USA). The transcripts were analyzed by using the comparative Ct method. β-actin was used as an internal control. The primer sequences were listed in Tables S5 and S6.

Proliferation, colony and spheroid formation

For cell proliferation measurement, cells were seeded into 24-well plates (2×10^4/well). Cell Counting Kit-8 solution was added 24, 48, 72, or 96 h after cell plating, and OD_{450} was measured by a plate reader. In the clonogeneicity assay, cells were seeded into 24-well plates (200/well) and cultured for 10–14 days with medium replacement for every three days. When the colonies reached the size visible to the naked eyes, they were fixed and stained with 1% crystal violet. Images were captured and the number of colonies was counted. In the spheroid formation assay, cells were seeded into Corning ultra-low attachment 24-well plates (2×10^4/well) and cultured in DMEM/F12 (1:1) medium supplemented with 2% B27, bFGF (20 ng/mL), and EGF (20 ng/mL) for 10–14 days. The number of spheroids was counted under microscope and the images were captured.

Transwell assay

Cell migration and invasion assays were assessed by modified Boyden chamber (Corning Costar, Rochester, NY, USA) containing a polycarbonate membrane filter with a pore size of 8.0 μm. For invasion assay, the upper chamber was pre-coated with Matrigel (Corning). 800 μL of medium containing 10% FBS was added to the lower chamber, 200 μL of cells (3×10^4 cells for migration and 5×10^4 cells for invasion) suspended in serum free medium were added to the upper chamber and incubated at 37°C in 5% CO_2 for 24 h. Cells remained on the top side of the membrane were gently removed, and those on the bottom surface were fixed and stained with 1% crystal violet. Images were captured by CellSens software under microscope at the magnification of 200×. The number of cells in each image was calculated by ImageJ software.

Enzyme linked immunosorbent assay (ELISA)

GB_{1e} or empty vector transfected MCF7 cells seeded into 96-well plates were fixed with 4% formaldehyde, permeabilized or not with 0.2% Triton X-100/PBS, blocked with 3% BSA/PBS, and sequentially incubated with primary antibody against Flag epitope and HRP-conjugated secondary antibody at room temperature (RT) for 30 min. The plates were washed followed by addition of enhanced chemiluminescence (ECL) reagents. The fluorescence signals were measured by FlexStation 3 (Molecular Devices, USA).

Immunoprecipitation

Cells were lysed with pre-cold IP buffer (20 mM Tris-HCl, pH 7.4, 150 mM NaCl, 1 mM EDTA, 1 mM EGTA, 1% Triton X-100, and 1% protease inhibitor cocktails) on ice for 20 min. 500 μg of total cell lysates (TCLs) were mixed with 20 μL of 4G10-conjugated agarose beads or EGFR antibody-conjugated sepharose beads

in a final volume of 500 μL and incubated overnight at 4°C with continuous agitation. In another set of IP experiments, 500 μg of TCLs were mixed with 2 μg of anti-PTPN12 or -Flag antibodies in a final volume of 500 μL and incubated overnight at 4°C with continuous agitation. 20 μL protein A/G-Sepharose beads were then added to each sample and incubated at 4°C for another 4 h. The beads were then washed, re-suspended in 2× electrophoresis loading buffer, and boiled for 10 min. The supernatants were subjected to immunoblotting or liquid chromatography-tandem MS (LC-MS/MS) analysis.

Immunoblotting

Immunoprecipitates, TCLs, condition medium, or tissue homogenates were resolved by SDS–PAGE followed by membrane transfer. Membranes were blocked, incubated with primary antibodies overnight at 4°C, and then probed with specific HRP-conjugated secondary antibodies at RT for 2 h. After extensive washing, the membranes were developed by ECL reagents.

Immunofluorescence

Cells seeded on coverslips (pre-coated with poly-lysine) placed in 12-well plates were cultured overnight and fixed with 4% formaldehyde at room temperature (RT) for 15 min. Afterwards, cells were rinsed, incubated with PBS in the presence or absence of 0.2% Triton X-100 for 5 min, and blocked with 3% BSA/PBS at RT for 30 min followed by incubating with primary antibody against GB_1 overnight at 4°C. Subsequently, cells were washed, incubated with appropriate Alexa Fluor 488-conjugated secondary antibody against mouse IgG at RT for 1 h, washed, stained with DAPI for 10 min, and washed again. The coverslips were mounted on glass slides and the images were acquired by FV10-ASW 3.1 Viewer under Olympus FV1000 microscope (Tokyo, Japan).

LC-MS/MS analysis

The TCLs from GB_{1e} or empty vector transfected MCF7 cells were immunoprecipitated with anti-Flag antibody, and the immunocomplex was resolved by SDS-PAGE followed by Coomassie Blue staining. Each lane was cut into four fragments and subjected to LC-MS/MS analysis.

Immunohistochemistry

Paraffin sections were incubated with 3% H_2O_2 to quench endogenous peroxidase activity, and then boiled in sodium citrate solution (10 mM, pH 6.0) to retrieve antigen. The slides were washed, blocked, and incubated with primary antibodies against GB_1, Ki-67, or pAkt overnight at 4°C followed by incubation with HRP-conjugated secondary antibodies at RT for 1 h. The slides were washed and stained with DAB detection kit (ZSGB-BIO, Beijing, China). The intensity of the immunostaining was quantified by using Image-Pro Plus 6.0 software.

Microsome isolation

Microsomes were isolated from MDA-MB-231 and MCF7-GB_{1e} cells by using a microsome isolation kit (Biovision, USA) according to manufacturer's instructions. Briefly, cells were washed once with 1 mL cold PBS and centrifuged. Then, the cell pellets were resuspended in cold homogenization buffer and transferred to pre-chilled Dounce homogenizer. The cell pellets were gently homogenized on ice followed by adding additional homogenization buffer to fully suspend homogenate. Afterwards, the homogenates were transferred to microcentrifuge tube, vortexed for 30 sec, incubated on ice for 1 min, and then centrifuged at 10,000 g for 15 min at 4°C. The supernatant was transferred to a new microcentrifuge tube and centrifuged at 20,000 g for 20 min at 4°C. The microsomal pellets were resuspended in cold PBS for further analysis. The purity and integrity of the microsomes were verified by the ratio of OD_{260}/OD_{280} (>1.8) and immunoblotting with ER marker calnexin.

Protease protection assays

The microsomes isolated from MDA-MB-231 and MCF-GB_{1e} cells were resuspended in PBS and treated or not with trypsin (100 μg/mL) and/or 1% Triton X-100 for 30 min on ice. The activity of trypsin was stopped by the addition of phenylmethylsulfonylfluoride to 1 mM (Schmitz et al., 2000).

Protein export assay

Twofold export buffer plus ATP (4 mM $MgCl_2$, 2 mM ATP, 20 mM creatine phosphate, 400 μg/mL creatine kinase in PBS, pH 7.5) or twofold export buffer minus ATP (4 mM $MgCl_2$, 50 mM glucose, 60 U/mL

hexokinase in PBS, pH 7.5) were added to microsomes resuspended in cold PBS. To analyze protein export in the presence of cytosol, microsomes were resuspended in 50% reticulocyte lysate plus ATP. All of the mixtures were incubated at 30°C for 20, 40, or 60 min followed by centrifugation (Schmitz et al., 2000).

Treat cells with $GABA_B$ receptor agonist

For cell proliferation assay, a total of 1×10^4 MCF7-V or MCF-GB_{1e} cells were seeded into 24-well plates and grown in complete DMEM for two days at 37°C with 5% CO_2. Cells were then incubated or not with $GABA_B$ receptor agonist baclofen (100 and 200 μM) or antagonist CGP54626 (5 and 10 μM) at 37°C for four consecutive days. The media were replaced every two days, and cell proliferation was examined every 24 h by using CCK-8 solution.

To examine the level of pAkt (S473), 4×10^5 of MCF7-V or MCF-GB_{1e} cells were seeded into 3.5-cm plates, maintained in complete DMEM for 2 days at 37°C with 5% CO_2 followed by serum starvation for 24 h. Cells were then incubated or not with baclofen (100 and 200 μM) or CGP54626 (5 and 10 μM) for 24 h at 37°C, and the TCLs were analyzed by immuoblot assay with antibodies against pAkt (S473), Akt, GB_1 and β-actin.

For clonogenic assay, 200 of MCF7-V or MCF-GB_{1e} cells were seeded into 24-well plates and treated or not with baclofen (100 and 200 μM) or CGP54626 (5 and 10 μM) for 10–14 days. The media were replaced every 3 days. When colonies were visible to the naked eyes, the plates were washed, fixed, and stained with 1% crystal violet. Images were captured and the number of colonies was counted.

QUANTIFICATION AND STATISTICAL ANALYSIS

Immunoblot results were quantitated by using ImageJ software, and the optical density of each band was normalized to β-actin. The data were presented as mean ± SEM. Statistical analyses were performed by using GraphPad Prism 8 software with one-way ANOVA with post hoc test (Tukey), paired or unpaired *t* test. *P* value less than 0.05 was considered statistically significant and the levels are indicated as: *p < 0.05, **p < 0.01, ***p < 0.001, ****p < 0.0001.